Geophysical Research Letters

RESEARCH LETTER
10.1029/2022GL099740

Hurricanes and Anomalous Heat in the Caribbean

Zack Guido[1,2], Teddy Allen[3], Simon Mason[4], and Pablo Méndez-Lázaro[5]

[1]Arizona Institutes for Resilient Environments and Societies, University of Arizona, Tucson, AZ, USA, [2]School or Natural Resources and Environment, University of Arizona, Tucson, AZ, USA, [3]Caribbean Institute for Meteorology and Hydrology, St. James, Barbados, [4]International Research Institute for Climate and Society, Earth Institute, Columbia University, Palisades, NY, USA, [5]Environmental Health Department, Graduate School of Public Health, University of Puerto Rico-Medical Campus, San Juan, Puerto Rico

Key Points:

- Areas around tropical cyclones have heat index (HI) values significantly warmer than average, a result insensitive to storm strength
- Positive HI anomalies occur after the cyclones passage in all storms; the maximum anomalies range from 0.3°C to 5.2°C
- Anomalous heat can be observed in areas 100s of kilometers away from the central location of the tropical storm

Supporting Information:

Supporting Information may be found in the online version of this article.

Correspondence to:

Z. Guido,
zguido@email.arizona.edu

Citation:

Guido, Z., Allen, T., Mason, S., & Méndez-Lázaro, P. (2022). Hurricanes and anomalous heat in the Caribbean. *Geophysical Research Letters*, *49*, e2022GL099740. https://doi.org/10.1029/2022GL099740

Received 26 MAY 2022
Accepted 19 OCT 2022

Author Contributions:

Conceptualization: Zack Guido, Teddy Allen, Simon Mason, Pablo Méndez-Lázaro
Formal analysis: Zack Guido, Teddy Allen, Simon Mason
Methodology: Zack Guido, Teddy Allen, Simon Mason
Writing – original draft: Zack Guido, Simon Mason
Writing – review & editing: Zack Guido, Teddy Allen, Simon Mason, Pablo Méndez-Lázaro

Abstract Co-occurring hazards present unparalleled challenges to development and disaster recovery. In this study, we investigate the relationship between anomalous heat in the aftermath of tropical cyclones in the eastern Caribbean between 1991 and 2020. We analyze the spatial patterns of anomalous heat index (HI) values for 53 tropical storms and hurricanes using a Lagrangian analysis framework. Furthermore, we analyze temporal patterns of 205 city-storms pairings. The spatial patterns displayed distinct and statistically significant areas of anomalously warm conditions regardless of the storm intensity classification. Moreover, all 205 city-storm events had positive HI anomalies following the storms' passage with a maximum of 5°C. The results show that HI anomalies can be high, have a time lag of days, and be observed in locations not directly impacted by the storm. The results have implications for tropical cyclones preparedness, including suggesting that preparedness include informing the public about heat impacts.

Plain Language Summary Two or more extreme events that are coincident in time or that occur in close succession present unparalleled challenges to development and disaster recovery. It is well known that tropical cyclones cause long-lived damage from strong winds, storm surges, intense rain, and/or flooding. Equally, heat is a main concern for public health. However, heat in the aftermath of tropical cyclones has not been a focus.We analyze 53 tropical storms and hurricanes in the eastern Caribbean between 1991 and 2020 and 205 storm-city events. The storms' heat index (HI) values are statistically significantly warmer during the storm than average in some regions, regardless of groupings of storms by their strength. The HI values before and after storms passed main cities in 14 Caribbean islands further show that in all 205 cases, warm HI anomalies follow the storms' passage, with values as high as 5°C (9 Fahrenheit). The results show that HI anomalies following tropical cyclones can be high, have maximums that occur several days after the storm's passage, and can be observed in locations that are not directly impacted by the storm. The results suggest tropical cyclone preparedness should include informing the public about heat risk.

1. Introduction

Hurricane Fiona first struck Puerto Rico on 18 September 2022. Three days later, an excessive heat advisory was issued by the National Weather Service for many regions on the island, including major population centers (Mercado, 2022). Tropical cyclones generate some of the costly disasters to society. In 2017 alone, tropical cyclones caused an estimated US$215B in damage (de Beurs et al., 2019). In isolation, tropical cyclones are major sources of vulnerability. The damages they create, however, can amplify the impacts of hazards that follow, like excessive heat (Cutter, 2018; Lawrence et al., 2020; Raymond et al., 2020).

Co-occurring hazards present unparalleled challenges to disaster recovery, development, and well-being (Aghakouchak et al., 2020; Zscheischler et al., 2018). Hurricanes Maria and Irma struck Puerto Rico in 2017 within 2 weeks of each other. Their immediate impacts contributed to excess mortality (Santos-Burgoa et al., 2018) and caused power outages that persisted for up to 11 months in some areas of Puerto Rico (Gould et al., 2018). The lack of energy left many households unable to cool their homes, refrigerate medications, or use essential medical equipment, thereby increased the risk of consequences to public health (Méndez-Lázaro et al., 2021; Ortiz et al., 2020). The impacts went even further, affecting tourism (Martín et al., 2020), agriculture (Rodríguez-Cruz & Niles, 2021), and the economy in general (Acosta et al., 2020; Martín et al., 2020).

It is common knowledge that tropical cyclones are accompanied by damaging winds, storm surges, intense rain, and flooding. Elevated heat-stress also occurs frequently as a meteorological precursor to hurricanes (Mercantini, 2002) and to flooding more generally (Zhang & Villarini, 2020). On the other hand, the presence and magnitude of heat following tropical storms have been analyzed only superficially. Matthews et al. (2019) analyzed hurricanes equivalent to a Category 3 or greater between 1979 and 2017. They assessed heat index (HI) values that exceeded 40.6°C in population centers within 30 days following the storm. However, excess mortality has been noted at HI values much lower than this (Burkart et al., 2011). Moreover, HI values in the Caribbean rarely exceed 35°C and, nonetheless, there is evidence that excess mortality occurs under elevated heat conditions (Méndez-Lázaro et al., 2021) and that heat is a main public health concern (Méndez-Lázaro, 2015; Méndez-Lázaro, Muller-Karger, et al., 2018; Méndez-Lázaro, Pérez-Cardona, et al., 2018; Méndez-Lázaro et al., 2021). Additionally, tropical cyclones can leave society more vulnerable to heat (Kozlov, 2021; Skarha et al., 2021), a risk that is increased by anthropogenic climate change (Feng et al., 2020; Gasparrini & Leone, 2014; Lin, 2019; Matthews et al., 2019).

In this study, we analyze the co-occurrence of tropical cyclones and heat in the Caribbean between 1991 and 2020, focusing on the temporal and spatial patterns of anomalous HI values. We also explore the temporal patterns of anomalous HI values across 14 islands that span the Lesser Antilles, excluding Trinidad and Tobago, but including Puerto Rico (shaded in red in Figure 1 and named in Table 1), hereafter referred to as the eastern Caribbean. We focus the timeseries analysis on the time after the passage of the tropical cyclone when compound impacts are likely to occur. This analysis has implications for how nations prepare for tropical cyclones, including calling attention to an important heat effect.

2. Setting

The Atlantic-Basin hurricane season extends from June through November when, on average, 14 named storms occur each year; seven of these reach hurricane strength and three become major hurricanes (NOAA, 2022). Hurricanes are the most damaging climate hazard to the region, often incurring annual costs to the region in excess of 100s of millions of dollars (Pielke et al., 2003). In St. Lucia, St. Kitts and Nevis, and Grenada, for example, hurricanes often generate economic losses greater than 5% of their gross domestic products (Guido et al., 2016). Low levels of gross domestic product relative to climate-adaptation costs further accentuate the vulnerability of Caribbean nations (Gould et al., 2018).

Our analysis spans the Eastern Caribbean, including Puerto Rico in the Greater Antilles but omitting Trinidad and Tobago. We exclude the large islands of Jamaican, Cuba, Hispaniola in the Greater Antilles and Trinidad and Tobago because their proximity to the other large islands and the landmasses of the United States and South America markedly influences the heat patterns in our spatial analysis.

Between 1991 and 2020, 53 tropical cyclones came within 100 km of the 14 islands used in this analysis (see methods; Figure 1). About 75% of these storms occurred in August and September during the peak of the seasonal temperature cycle.

3. Data and Methods

We obtained North Atlantic tropical cyclone track-data from the International Best Track Archive for Climate Stewardship (IBTrACS) data set (Knapp et al., 2010). The IBTrACS data include the best estimate of the latitude and longitude of the center of each storm at 3-hr intervals. We selected all storms of tropical storm strength or greater between 1991 and 2020 whose center of low pressure passed within 100 km of the capital city of the 14 islands listed in Table 1. These criteria produced a data set of 53 unique cyclones that generated 205 cyclone-city events. We show the storm tracks of all storms in Figure 1 and a list of characteristics of each storm in the Table S1 in Supporting Information S1.

Heat index values were calculated using the Copernicus Climate Change Service (C3S) European Centre for Medium-Range Weather Forecasts Reanalysis (ERA5) hourly 0.25° latitude-longitude High Resolution (HRES) data (Hersbach et al., 2020). The HI was calculated using Rothfusz's (1990) simplification of Steadman (1979) heat-stress index. Although Rothfusz's index is calculated using only the dry-bulb temperature and relative humidity, the index can be interpreted as a complex expression of how heat is experienced physiologically

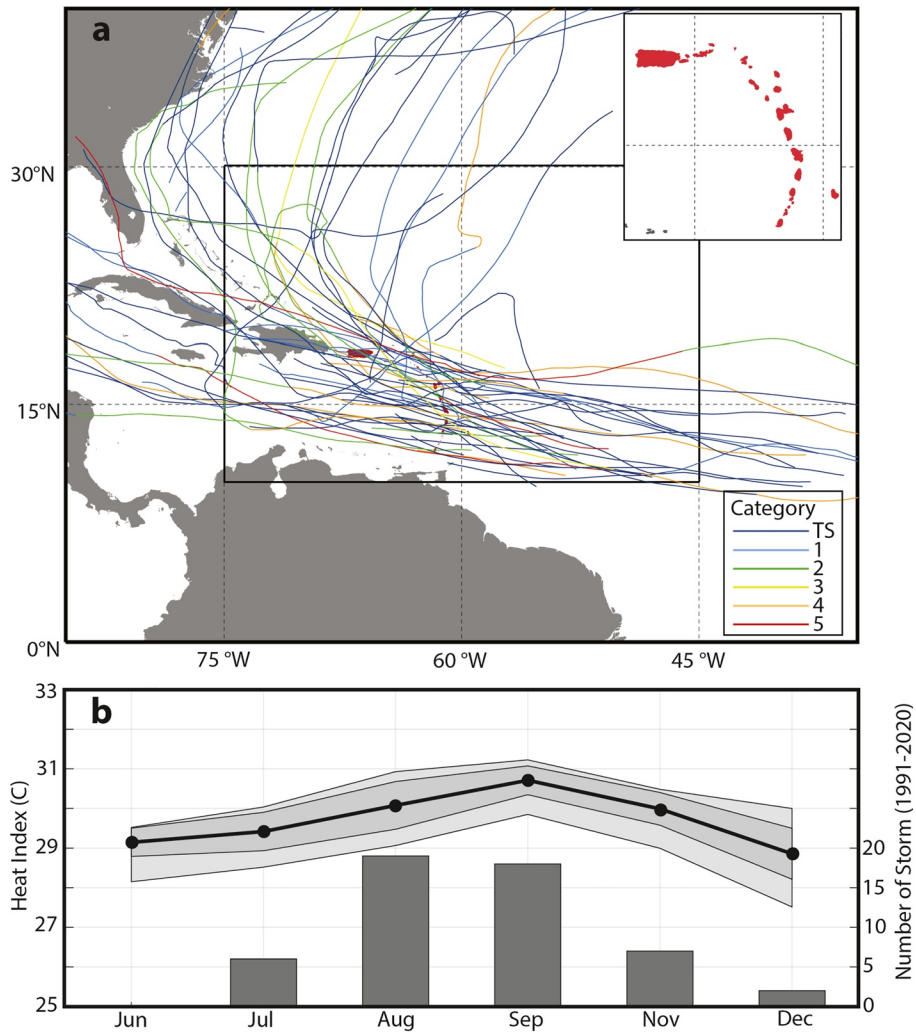

Figure 1. (a) Storm tracks for 53 tropical cyclones and hurricanes between 1991 and 2020. The islands used for selecting the storms are in the top right inset. The box in the center indicates the domain used for the Lagrangian analysis: storms were tracked when their center was within this box. (b) The frequency of occurrence of the 53 tropical cyclones analyzed (bars) along with the monthly average heat index (black lines/circles). The lighter gray shading represents the minimum and maximum average monthly values; the darker gray shading represents the standard deviation of the average monthly values.

(Rothfusz, 1990). The ERA5 2-m temperature data were used as the dry-bulb temperature (T) in Rothfusz's equation:

$$\begin{aligned} \mathrm{HI} = &-42.379 + 2.04901523 \times T + 10.14333127 \times \mathrm{RH} - 0.22475541 \times T \times \mathrm{RH} \\ &-6.83783 \times 10^{-3} \times T^2 - 5.481717 \times 10^{-2} \times \mathrm{RH}^2 + 1.22874 \times 10^{-3} \times T^2 \times \mathrm{RH} \\ &+8.5282 \times 10^{-4} \times T \times \mathrm{RH}^2 - 1.99 \times 106 \times T^2 \times \mathrm{RH}^2 \end{aligned} \quad (1)$$

The 2-m relative humidity, RH, was calculated from the ERA5 dry-bulb and dew-point temperatures (T and T_d, respectively, and both in °C) using:

$$\mathrm{RH} = 100\,\mathrm{x}\,\exp(17.625\mathrm{Td} / 243.04 + \mathrm{Td}) / \exp(17.625\mathrm{T} / 243.04 + \mathrm{T}) \quad (2)$$

RH is accurate to within 0.4% for realistic temperatures in the Caribbean (M. G. Lawrence, 2005).

To identify the spatial structure and possible causes of anomalous heat associated with a tropical cyclone's passage, we conducted a Lagrangian analysis of the HI over a spatial domain of a 20° × 20°. This domain encap-

Table 1
Descriptive Statistics Aggregated by Country for Anomalies and Values (in Parentheses) for the 5-Day Period After the Cyclones' Closest Position to Each Country's Capital City

Country and capital	Storms #	Lowest max. (°C)	Avg. max. (°C)	Highest max. (°C)	Avg. median (°C)	Avg. IQR (°C)	Avg. timing maximum Hrs [range hrs]
Grenada, St. Georges	7	1.7 (31.49)	2.1 (32.3)	2.9 (33.7)	0.2 (30.6)	−0.8 to +1.0 (29.3–31.2)	52.7 [27–87]
Barbados, Bridgetown	12	1.4 (30.6)	1.9 (32.0)	2.3 (32.9)	0.2 (30.4)	−0.7 to +0.9 (29.4–31.0)	52.6 [15–120]
Saint Vincent, Kingstown	11	1.4 (30.5)	2.1 (32.3)	3.0 (33.1)	0.2 (30.7)	−0.8 to +1.0 (29.4–31.2)	42.6 [15–114]
Saint Lucia, Castries	17	1.2 (32.7)	2.0 (34.4)	3.0 (36.9)	−0.1 (29.6)	−0.9 to +0.6 (28.0–31.5)	61.0 [9–118]
Martinique, Fort-du-France	14	0.9 (30.0)	1.9 (31.5)	2.9 (32.7)	0.1 (29.7)	−0.8 to +0.8 (28.6–30.4)	50.4 [2–120]
Dominica, Roseau	13	0.7 (29.9)	1.6 (31.6)	2.7 (32.8)	0.2 (30.3)	−0.8 to +0.8 (28.9–30.6)	69.8 [25–120]
Guadeloupe, Les Abymes	16	0.9 (30.0)	2.0 (32.1)	3.1 (33.4)	−0.1 (29.0)	−1.1 to +0.7 (27.9–30.0)	60.1 [1–110]
Montserrat, Brades	18	0.3 (28.4)	1.7 (32.0)	2.5 (33.6)	−0.1 (30.4)	−1.0 to +0.6 (29.2–31.0)	43.4 [2–88]
Antigua, St. John	14	0.3 (28.6)	1.8 (32.2)	3.0 (34.3)	0.0 (30.7)	−0.9 to +0.7 (29.5–31.1)	40.9 [3–101]
Saint Kitts, Basseterre	17	0.8 (30.5)	1.9 (32.2)	3.4 (33.4)	−0.2 (30.3)	−1.0 to +0.6 (29.2–30.9)	52.1 [1–120]
Saint Martin, Margot	15	0.8 (28.2)	2.0 (32.2)	4.0 (35.7)	−0.1 (30.2)	−1.0 to +0.6 (29.2–30.9)	47.3 [7–119]
Anguilla, Sandy Point	17	0.8 (28.2)	2.0 (32.1)	4.1 (35.7)	−0.1 (30.1)	−1.0 to +0.7 (29.1–30.8)	42.8 [3–119]
Puerto Rico, San Juan	15	1.1 (31.1)	2.8 (36.3)	5.2 (39.5)	−0.2 (29.4)	−1.5 to +0.7 (27.3–31.7)	60.3 [21–120]
British Virgin Is., Road Town	19	0.9 (28.3)	1.9 (32.6)	3.5 (35.2)	0.1 (31.1)	−0.9 to +0.9 (29.6–31.5)	43.2 [2–114]
Grand Avg [Total]	[205]	0.9 (29.9)	2.0 (32.6)	3.2 (34.5)	0.0 (30.2)	−0.9 to +0.7 (28.9–31.0)	51.0

Note. The final column refers to the number of hours after the storm's passage in which each cyclone's maximum heat index anomaly occurred. IQR: interquartile range.

sulates the entire spatial footprint of the tropical cyclones (assessed by inspecting wind vectors). In the Lagrangian analysis, the reference point is always centered on the core of the storm, and the 20° × 20° grid is adjusted accordingly at each 3-hr interval. The HI values for each grid and for each time were converted to anomalies using a 30-day average of the corresponding hour of day. The 30-values included the 15 prior to the corresponding hour, the corresponding hour, and 14 that followed it. Over the duration of the storm, we averaged the HI anomalies at each grid point. We also averaged the 10-m u- and v-wind components of the ERA5 data at each grid to help assess possible pathways for heat advection. We restricted the cyclones duration to be when a storm's center is located within the central box of Figure 1. The cyclones' effects on the HI are considered only when their center is within the vicinity of the eastern Caribbean; HI values are calculated for the entire 20° × 20° domain surrounding the cyclone center.

Time series of HI anomalies were constructed for each storm affecting each island state, producing 205 series. We calculated the distance from the capital city of each island for each 3-hr interval using Vincenty's (1975) formula under the assumption of a spherical earth. The time-series covered a 30-day window centered on the date that the storm's center was closest to the island states' respective capital city. The HI values for each hour were converted to anomalies with respect to the 30-day average of the corresponding hour of day centered in time when the storm is closest to the city. This procedure provides an indication of the relative HI for the 360 hr (15 days prior to and after a storm's passage). Anomalies facilitate comparisons among the storms, simplify the identification of relative peaks in HI associated with the passage of a tropical cyclone, and enable the creation of country composites. Additionally, the anomalies account for differences in warmer or cooler years and for any differences in HI climatology during the hurricane season.

There are several caveats for the timeseries analysis. The 15-day pre-storm period of Hurricane Maria in 2017 completely overlaps with the 15-day post-storm period of an earlier storm Hurricane Irma. The effect of the overlap on the anomaly in the composites is minimal and would reflect a slight dampening of pre- and post-storm heat signals. Second, there are differences in the average monthly HI values during the North Atlantic hurricane season (Figure 1b). However, the differences between any two 30-day averages are small compared to the day-to-day variability. We chose to ignore the seasonal cycle for the purposes of calculating the 30-day averages. The effect of not accounting for the seasonal cycle is to slightly underestimate the relative magnitude of any

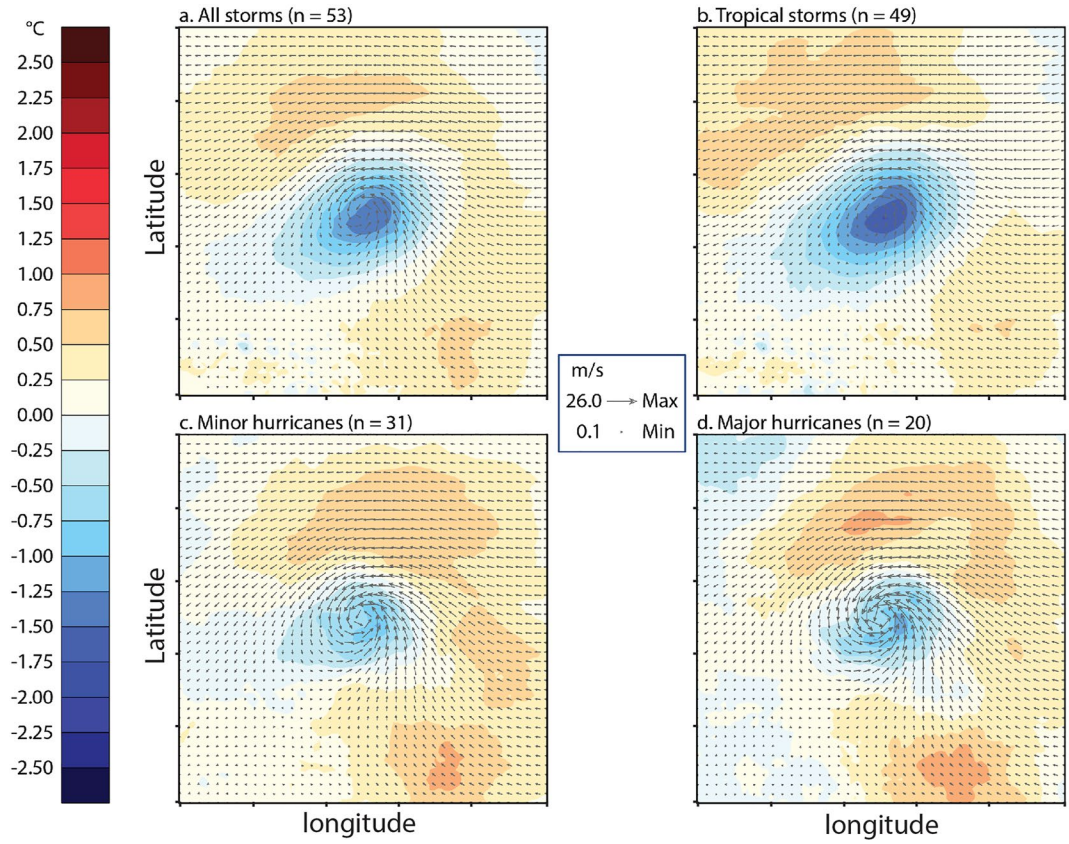

Figure 2. Spatial pattern of heat index (HI) anomalies for (a) all 53 cyclones, (b) only tropical storms, (c) minor hurricanes of categories 1–3 and (d) major hurricanes of categories 4–5. The spatial domain is 20° × 20°. "n" refers to the number of unique storms contributing to the composite. The HI anomalies are first averaged over time for each storm at the specified strengths in panels a–d, and then averaged across all storms so that each storm has equal weight.

post-cyclone heat events. Finally, using a 30-day average inflates the daily HI anomalies in the first 15 days more so than the second 15 days prior to September when daily temperatures are increasing. After September, when daily temperatures decline, the HI anomalies for the second 15 days are elevated relative to the first 15 days. These final two conditions likely cause our HI anomalies to be slightly underestimated following the cyclones passage of the reference city.

4. Results

4.1. Spatial Heat Index Anomaly Patterns

Figure 2a shows averaged anomalous HI values for the 53 storms when the center of low pressure is within the central box indicated in Figure 1. The averaged wind direction also show that the anomalous heat is within the storms' circulation. The HI anomalies are first averaged over time for each storm at the specified magnitude in the groupings, and then averaged across all storms so that each storm is given equal weight. Separate results are shown for storm strength groupings. In this way, Hurricane Maria in 2017, for example, has spatial patterns that are averaged in each of the four composites because it varied from tropical storm to hurricane strength category 5 within the analyzed domain.

For all storm intensities, the main spatial features are the central core of anomalously low heat due to storm related cloud cover and a surrounding area of anomalously high heat in an arc extending from the south south-east of the storm center to the north-west. Across the groupings, the arc pattern is similar. The location of highest HI values is generally northwest and southeast of the storms' center. The peak values, however, are higher for more intense storm groupings.

The standard deviations of the average HI across the storms in most cases are 0.5–1.0°C. Based on a one-tailed, one-sample *t*-test, the average temperature anomalies are significantly larger than zero ($\alpha = 0.05$) when the anomaly exceeds between about 0.25 and 0. 50°C (Figure S1 in Supporting Information S1). These p-value calculations are likely to be conservative because the degrees of freedom have been defined by the number of storms rather than by the number of time steps to be consistent with giving each storm equal weight. In all four composites, the areas of anomalously high heat to the north and northwest and to the southeast indicate areas of statistically significant heating.

Anomalously high HI values around the storms span about 3–8 degrees of latitude and longitude. Given this reach, an island can experience anomalous heat even if the storm passes 100s of km from its coast. The heat patterns also indicate an effect of storm tracks on the heat experienced at a location. Most of the storms move in a westward to north-westward direction. Therefore, anomalous heat may be experienced prior to a storm if the storm approaches from the south-east, and after a storm if the storm continues to track to the north-west. For minor and major hurricanes, a trajectory passing south of an island and moving in a north-westerly direction could lead to, on average, lower and less persistent anomalous heat post storm than if the storm passed to the west of the island. Given this sensitivity to storm track, it is of interest to consider how anomalous heat is experienced at specific locations.

4.2. Temporal Heat Index Anomaly Patterns in the Wake of Cyclones

During the 30-year period, the 53 tropical cyclones produced 205 city-storm events. The trajectory of the cyclone affects the number of islands it impacts. Hurricane Marilyn in 1995 came within 100 miles of nine countries, while that same year tropical storm Sebastien affected only one country. In the 5 days following a cyclone's passage, the average maximum HI anomaly ranged between 1.6°C and 2.1°C for all countries except for Puerto Rico, which had an average maximum anomaly value of 2.8°C. Table 1 presents summary statistics for the countries.

All countries experienced periods of anomalously high HI values in the wake of a storm. Table 1 presents descriptive statistics summarized at the country level for a 5-day period following the storms. The peak in the maximum HI anomaly values was or exceeded 3°C for 9 of the 14 capitals. Puerto Rico had the highest maximum HI anomaly at more than 5.2°C. The peak in anomalous HI value occurred most often within 3 days, particularly for hurricanes (Figure 3b); the peak for major hurricanes was often within the first day. The number of hours after the storm's passage in which peak HI anomalies occurred had considerable variability that was influenced by the speed of the storm.

The timing and degree of any HI anomaly is affected by a storm track and distance (as implied in Figure 2) as well as its size, speed, and the background climate through which the storm moves. As a result, each storm has a unique temporal pattern. However, a grand composite of all 30-day time series illustrates a typical temporal heat pattern as storms approach and move away from a reference location (Figure 3). The composite time-series shows three defining features. First, 1–2 days prior to the passage of the storm, anomalous HI values are highest. Second, a large decrease in the anomalous heat is then concurrent with the storm's closest position. Finally, in the wake of the storm, anomalous heat peaks within 2 days of the storms' passage, albeit at a lower value than the peak prior to the storm's passage.

There is high variability across island time-series and from event to event at a singular location, and thus a post-storm heat anomaly can be suppressed in the mean and standard deviation composites shown in Figure 3a. Accounting for the speed of the storms using distance instead of time on the *x*-axis shows a similar pattern (Figure S2 in Supporting Information S1). Major hurricanes on average have a higher maximum anomalous HI, a greater interquartile range of the maximum HI anomaly, and a longer time lag in which the maximum HI anomalies occur after the hurricane's passage compared to tropical storms and minor hurricanes (Figures 3b and 3c).

The two highest maximum values across all islands and storms occurred in Puerto Rico during Hurricane Dorian (2019) and Hurricane Marilyn (1995), approximately 55 and 47 hr after the storm's closest passage to San Juan, respectively. In both cases, the higher values are localized to the island's landmass (Figures S3 and S4 in Supporting Information S1). A visual inspection of the spatial patterns around the time of peak warming for Puerto Rico for the six storms with maximum HI anomalies greater than 3°C also shows a similar hotspot feature over the

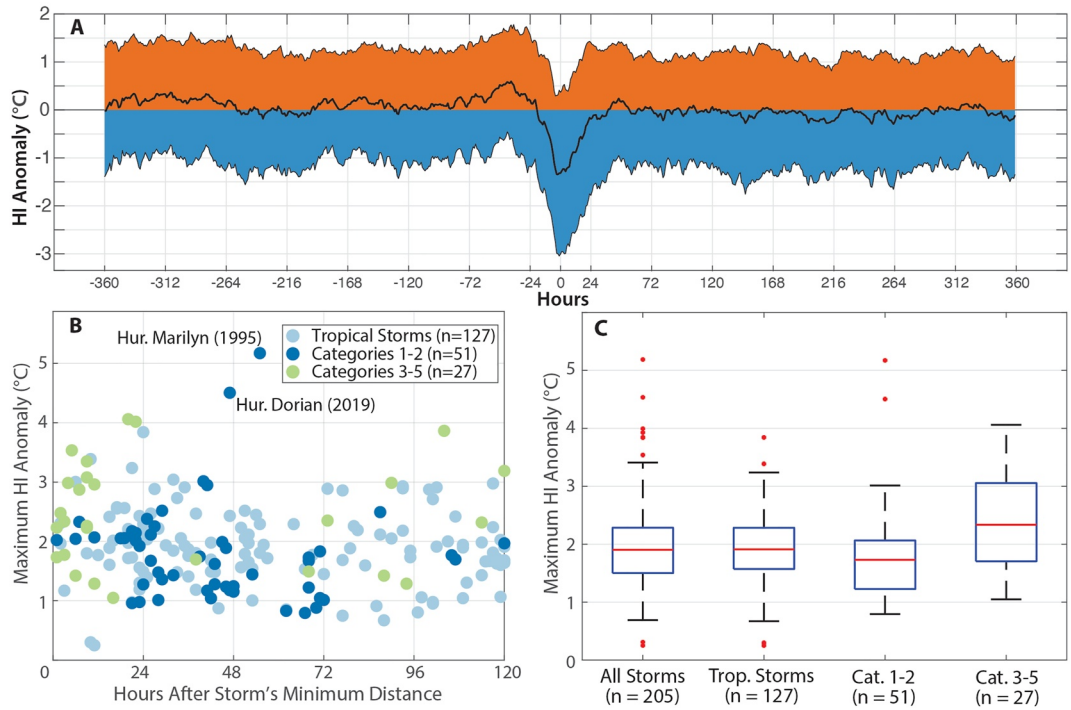

Figure 3. (a) Time-series of heat index (HI) anomalies for all 205 country-events. Shaded area is a 1 standard deviation range; black line is the mean HI for each hour of all 205 country-events. Hour zero denotes the storm's closest distance to the reference city, with negative and positive hours occurring before and after that time, respectively. (b) Scatter plot of post-storm peak anomalous HI by hour colored by strength. (c) Distributions of the maximum HI anomalies for all storms (left box plot) and for storm strength categories (3 right boxplots). Storms were classified into S/S categories based on the wind speed at the closest distance to the reference city. The number of values in each distribution is given on the *x*-axis (e.g., $n = 127$).

land. Smaller islands do not have as prominent of a hotspot, suggesting land-surface effects may amplify the heat. The lack of the hotspot over smaller islands could also relate to data resolution.

5. Discussion and Conclusion

We emphasize the following results. First, the spatial patterns of HI values show distinct and statistically significant areas of anomalously warm conditions regardless of the storm intensity classification (Figure 1; Figure S1 in Supporting Information S1). Positive HI anomalies occur north, east, and south of the low center. These patterns are similar for composites of different storm strengths. Second, anomalous HI values were experienced after the passage of a cyclone in each of the 205 city-storm events, some as much as 5°C (Table 1). Moreover, the ERA5 data likely underestimate these anomalies as the median difference between temperatures measured at stations in the reference cities and the corresponding ERA5 grid was about 1°C (Figure S4 in Supporting Information S1). The peak in heat prior to the storms passage merits further inquiry; it may impact public health during the preparatory phase for an oncoming cyclone. Third, the intensity and timing of the peak anomalous heat exhibits high variability in part because of the speed and track of each storm. Finally, the spatial footprints of tropical cyclone-related warming are large and on average observed 100s of kilometers away from the cyclones' center. Thus, positive heat anomalies can occur after a lag of days and in locations that do not receive the brunt of a storm's impacts.

We suggest three main mechanisms to explain the spatial heat pattern in Figure 2: heat transport, subsidence of air around the cyclone, and solar radiation. Heat transport is influenced by the circulation of the storm and the meridional temperature gradient. The anomalously warm conditions on the southern side of the cyclone, and in particular the southeast quadrant of Figure 2, would be influenced by warmer and moist air advected in from the south. Likewise, the cooler conditions to the west of the storm would be influenced by cooler air transported from

the north. Moving away from the center of the cyclone, persistent areas of aior subsidence would lead to adiabatic warming, while also influencing cloud shading. Higher insolation would occur in areas with lower cloud cover, itself influenced by subsidence. The degree to which each of these mechanisms can explain the heat pattern requires further study.

The question arises as to whether a positive HI anomaly of several degrees C is consequential. Such a nuanced question requires attention to thermal comfort and socio-economic conditions at a level beyond the scope of this paper. We also note that our results based on gridded data may underestimate the heat observed on the ground. Nonetheless, research suggests that changes of several degrees are impactful on public health outcomes in several ways. First, several studies show increases in excess mortality per unit change in heat. In the United States, Bobb et al. (2014) estimated an excess of 1,907 deaths per summer per a 2.8°C (5°F) increase in average daily temperatures, while Burkart et al. (2011) showed that mortality in rural and urban areas in Bangladesh increased between 2.4% and 3.9% for a 1°C increase in HI. In the latter study, mortality began to increase at HI thresholds around 31°C, around the values we present in Table 1. Second, uncomfortable temperatures in the aftermath of Hurricane María were among the top concerns of cancer patients and health-care providers and administrators (Méndez-Lázaro et al., 2021). Finally, Bobb et al. (2014) showed that larger increases in central air conditioning prevalence tended to have slightly larger reductions in heat-related mortality risk over time. This implies that in the absence of electricity to power air conditioning, which would occur in the wake of damaging cyclones, excess mortality may increase.

Damaging winds and floods are the dominant impacts from tropical cyclones. Emergency management is focused on anticipating and addressing impacts from these forces. This research has identified a spatial pattern of anomalous heat that is also associated with tropical cyclones and it generates at times large positive heat anomalies. We therefore call attention to a compound environmental stressor not well-appreciated: heat and hurricanes. Global warming only elevates the need to recognize the dual impacts from tropical cyclones and heat.

It is our hope that this analysis instigates studies that explicitly link compound heat and hurricanes conditions to public health impacts. Even in absent of more research, there is evidence to alert people to prepare for warmer-than-average conditions after storms. We suggest that emergency managers and national weather services who are charged with public communication and preparedness activities consider communicating about potential heat impacts in the wake of potentially devastating storms.

Data Availability Statement

The IBTrACS data can be accessed at https://ibtracs.unca.edu/index.php?name=browse-year-basin. The ERA5 hourly data can be accessed at https://cds.climate.copernicus.eu/cdsapp#!/dataset/reanalysis-era5-single-levels?tab=form.

Acknowledgments
The IBTrACS is publicly available from the U.S. National Oceanic and Atmospheric Administration (see Knapp et al., 2010). The ERA5 HRES data is publicly available from the ECMWF (see Hersbach et al., 2020). This work was supported through a grant from the National Oceanic and Atmospheric Administration International Research and Applications Project (NA18OAR4310338).

References

Acosta, R. J., Kishore, N., Irizarry, R. A., & Buckee, C. O. (2020). Quantifying the dynamics of migration after Hurricane Maria in Puerto Rico. *Proceedings of the National Academy of Sciences of the United States of America*, *117*(51), 32772–32778. https://doi.org/10.1073/pnas.2001671117

Aghakouchak, A., Chiang, F., Huning, L. S., Love, C. A., Mallakpour, I., Mazdiyasni, O., et al. (2020). Climate extremes and compound hazards in a warming world. *Annual Review of Earth and Planetary Sciences*, *48*(1), 519–548. https://doi.org/10.1146/annurev-earth-071719-055228

Bobb, J. F., Peng, R. D., Bell, M. L., & Dominici, F. (2014). Heat-related mortality and adaptation to heat in the United States. *Environmental Health Perspectives*, *122*(8), 811–816. https://doi.org/10.1289/ehp.1307392

Burkart, K., Schneider, A., Breitner, S., Khan, M. H., Krämer, A., & Endlicher, W. (2011). The effect of atmospheric thermal conditions and urban thermal pollution on all-cause and cardiovascular mortality in Bangladesh. *Environmental Pollution*, *159*(8–9), 2035–2043. https://doi.org/10.1016/J.ENVPOL.2011.02.005

Cutter, S. L. (2018). Compound, cascading, or complex disasters: What's in a name? *Environment: Science and Policy for Sustainable Development*, *60*(6), 16–25. https://doi.org/10.1080/00139157.2018.1517518

de Beurs, K. M., McThompson, N. S., Owsley, B. C., & Henebry, G. M. (2019). Hurricane damage detection on four major Caribbean islands. *Remote Sensing of Environment*, *229*, 1–13. https://doi.org/10.1016/j.rse.2019.04.028

Feng, K., Min, O., & Lin, N. (2020). Hurricane-blackout-heatwave compound hazard risk and resilience in a changing climate. Retrieved from https://arxiv.org/abs/2012.04452v1

Gasparrini, A., & Leone, M. (2014). Attributable risk from distributed lag models. *BMC Medical Research Methodology*, *14*(1), 55. https://doi.org/10.1186/1471-2288-14-55

Gould, W. A., Díaz, E. L., Álvarez-Berríos, N. L., Aponte-González Aponte, F., Wayne Archibald, A., Heath Bowden, J., et al. (2018). 2018: U.S. Caribbean. In D. R. Reidmiller, C. W. Avery, D. R. Easterling, K. E. Kunkel, K. L. M. Lewis, T. K. Maycock, et al. (Eds.), *Impacts, risks, and adaptation in the United States: Fourth national climate assessment, volume II* (Vol. 2, pp. 809–871). U.S. Global Change Research Program. https://doi.org/10.7930/NCA4.2018.CH20

Guido, Z., Rountree, V., Greene, C., Gerlak, A., & Trotman, A. (2016). Connecting climate information producers and users: Boundary organization, knowledge networks, and information brokers at Caribbean climate outlook forums. *Weather, Climate, and Society*, *8*(3), 285–298. https://doi.org/10.1175/WCAS-D-15-0076.1

Hersbach, H., Bell, B., Berrisford, P., Hirahara, S., Horányi, A., Muñoz-Sabater, J., et al. (2020). The ERA5 global reanalysis. *Quarterly Journal of the Royal Meteorological Society*, *146*(730), 1999–2049. https://doi.org/10.1002/qj.3803

Knapp, K. R., Kruk, M. C., Levinson, D. H., Diamond, H. J., & Neumann, C. J. (2010). The international best track archive for climate stewardship (IBTrACS). *Bulletin of the American Meteorological Society*, *91*(3), 363–376. https://doi.org/10.1175/2009BAMS2755.1

Kozlov, M. (2021). Hurricane Ida forces Louisiana researchers to rethink their future. *Nature*, *597*(7876), 313–314. https://doi.org/10.1038/d41586-021-02456-z

Lawrence, J., Blackett, P., & Cradock-Henry, N. A. (2020). Cascading climate change impacts and implications. *Climate Risk Management*, *29*, 100234. https://doi.org/10.1016/j.crm.2020.100234

Lawrence, M. G. (2005). The relationship between relative humidity and the dewpoint temperature in moist air: A simple conversion and applications. *Bulletin of the American Meteorological Society*, *86*(2), 225–234. https://doi.org/10.1175/BAMS-86-2-225

Lin, N. (2019). Tropical cyclones and heatwaves. *Nature Climate Change*, *9*(8), 579–580. https://doi.org/10.1038/s41558-019-0537-2

Martín, Y., Cutter, S. L., Li, Z., Emrich, C. T., & Mitchell, J. T. (2020). Using geotagged tweets to track population movements to and from Puerto Rico after Hurricane Maria. *Population and Environment*, *42*(1), 4–27. https://doi.org/10.1007/s11111-020-00338-6

Matthews, T., Wilby, R. L., & Murphy, C. (2019). An emerging tropical cyclone–deadly heat compound hazard. *Nature Climate Change*, *9*(8), 602–606. https://doi.org/10.1038/s41558-019-0525-6

Méndez-Lázaro, P. A. (2015). Extreme heat events in San Juan Puerto Rico: Trends and variability of unusual hot weather and its possible effects on ecology and society. *Journal of Climatology & Weather Forecasting*, *03*(02), 1000135. https://doi.org/10.4172/2332-2594.1000135

Méndez-Lázaro, P. A., Bernhardt, Y. M., Calo, W. A., Pacheco Díaz, A. M., García-Camacho, S. I., Rivera-Lugo, M., et al. (2021). Environmental stressors suffered by women with gynecological cancers in the aftermath of Hurricanes Irma and María in Puerto Rico. *International Journal of Environmental Research and Public Health*, *18*(21), 11183. https://doi.org/10.3390/ijerph182111183

Méndez-Lázaro, P. A., Muller-Karger, F. E., Otis, D., McCarthy, M. J., & Rodríguez, E. (2018). A heat vulnerability index to improve urban public health management in San Juan, Puerto Rico. *International Journal of Biometeorology*, *62*(5), 709–722. https://doi.org/10.1007/s00484-017-1319-z

Méndez-Lázaro, P. A., Pérez-Cardona, C. M., Rodríguez, E., Martínez, O., Taboas, M., Bocanegra, A., & Méndez-Tejeda, R. (2018). Climate change, heat, and mortality in the tropical urban area of San Juan, Puerto Rico. *International Journal of Biometeorology*, *62*(5), 699–707. https://doi.org/10.1007/s00484-016-1291-z

Mercado, A. (2022). Puerto Ricans now face heat wave after days without power and water. Retrieved from https://gizmodo.com/puerto-rico-hurricane-fiona-heat-wave-blackout-1849563984

Mercantini, J. (2002). The great Carolina Hurricane of 1752 on JSTOR. *South Carolina Historical Magazine*, *103*(4), 351–365. Retrieved from https://www.jstor.org/stable/27570598?seq=1#metadata_info_tab_contents

NOAA. (2022). Tropical cyclone climatology. Retrieved from https://www.nhc.noaa.gov/climo/

Ortiz, A. P., Calo, W. A., Mendez-Lazaro, P. A., García-Camacho, S., Mercado-Casillas, A., Cabrera-Márquez, J., & Tortolero-Luna, G. (2020). Strengthening resilience and adaptive capacity to disasters in cancer control plans: Lessons learned from Puerto Rico. *Cancer Epidemiology, Biomarkers & Prevention*, *29*(7), 1290–1293. https://doi.org/10.1158/1055-9965.EPI-19-1067

Pielke, R. A., Rubiera, J., Landsea, C., Fernández, M. L., & Klein, R. (2003). Hurricane vulnerability in Latin America and the Caribbean: Normalized damage and loss potentials. *Natural Hazards Review*, *4*(3), 101–114. https://doi.org/10.1061/(asce)1527-6988(2003)4:3(101)

Raymond, C., Horton, R. M., Zscheischler, J., Martius, O., AghaKouchak, A., Balch, J., et al. (2020). Understanding and managing connected extreme events. *Nature Climate Change*, *10*(7), 611–621. https://doi.org/10.1038/s41558-020-0790-4

Rodríguez-Cruz, L. A., & Niles, M. T. (2021). Awareness of climate change's impacts and motivation to adapt are not enough to drive action: A look of Puerto Rican farmers after Hurricane Maria. *PLoS One*, *16*(1), e0244512. https://doi.org/10.1371/journal.pone.0244512

Rothfusz, L. P. (1990). *The heat index equation (or, more than you ever wanted to know about heat index)*. National Oceanic and Atmospheric Administration, National Weather Service, Office of Meteorology. Retrieved from http://www.paper/c6bd9143-3623-4d4f-963f-62942ed32f11/Paper/p395

Santos-Burgoa, C., Sandberg, J., Suárez, E., Goldman-Hawes, A., Zeger, S., Garcia-Meza, A., et al. (2018). Differential and persistent risk of excess mortality from Hurricane Maria in Puerto Rico: A time-series analysis. *The Lancet Planetary Health*, *2*(11), e478–e488. https://doi.org/10.1016/S2542-5196(18)30209-2

Skarha, J., Gordon, L., Sakib, N., June, J., Jester, D. J., Peterson, L. J., et al. (2021). Association of power outage with mortality and hospitalizations among Florida nursing home residents after hurricane Irma. *JAMA Health Forum*, *2*(11), e213900. https://doi.org/10.1001/jamahealthforum.2021.3900

Steadman, R. G. (1979). The assessment of sultriness. Part I. A temperature-humidity index based on human physiology and clothing science. *Journal of Applied Meteorology*, *18*(7), 861–873. https://doi.org/10.1175/1520-0450(1979)018<0861:TAOSPI>2.0.CO;2

Vincenty, T. (1975). Direct and inverse solutions of geodesics on the ellipsoid with application of nested equations. *Survey Review*, *23*(176), 88–93. https://doi.org/10.1179/sre.1975.23.176.88

Zhang, W., & Villarini, G. (2020). Deadly compound heat stress-flooding hazard across the Central United States. *Geophysical Research Letters*, *47*(15), e2020GL089185. https://doi.org/10.1029/2020GL089185

Zscheischler, J., Westra, S., Van Den Hurk, B. J. J. M., Seneviratne, S. I., Ward, P. J., Pitman, A., et al. (2018). Future climate risk from compound events. *Nature Climate Change*, *8*(6), 469–477. https://doi.org/10.1038/s41558-018-0156-3